

## NUMERICAL ANALYSIS OF ROTORDYNAMIC COEFFICIENTS OF ANNULAR FLOW IN CANNED MOTOR RCP

### Yaoyu Hu

School of Mechanical Engineering  
Shanghai Jiao Tong University  
Shanghai, China  
Email: huyaoyu@sjtu.edu.cn

### Dezhong Wang

School of Mechanical Engineering  
Shanghai Jiao Tong University  
Shanghai, China  
Email: dzwang@sjtu.edu.cn

### Junlian Yin

School of Mechanical Engineering  
Shanghai Jiao Tong University  
Shanghai, China  
Email: jlyin@sjtu.edu.cn

### Yujin Wang

School of Mechanical Engineering  
Shanghai Jiao Tong University  
Shanghai, China  
Email: battlestar@sjtu.edu.cn

### ABSTRACT

*The operating performance and safety characteristics of canned motor Reactor Coolant Pump (RCP) are vital to the nuclear reactor. The annular flow, which is between the rotor and stator, makes substantial effects on the rotordynamic characteristics of RCP. In this work, the annular flow is simulated by means of 3-dimensional CFD approaches. The annular flow field and the auxiliary impeller are modeled. The results show that the pre-swirl strength at the inlet of the annular flow is evident. Another model without the auxiliary impeller is analyzed under constant pre-swirl ratio with various axial flow rates and whirl speeds. The rotordynamic coefficients of the annular flow are obtained. The results are compared with theoretical predictions. Numerical results show that the fluid in the annular region makes remarkable effects on the rotordynamic characteristics of the canned motor RCP.*

### NOMENCLATURE

$C$  direct damping coefficient (Ns/m)  
 $c$  cross-coupled damping coefficient (Ns/m)  
 $d$  diameter of the rotor (m), in Tab. 1

$e$  eccentricity of the rotor center  
 $F_x$  force component along  $x$ -axis (N)  
 $F_z$  force component along  $z$ -axis (N)  
 $f_n$  normal force component (N)  
 $f_t$  tangential force component (N)  
 $H$  clearance defined in Eqn. (5) (m)  
 $h$  nominal clearance (m),  $h = r_2 - r_1$   
 $K$  direct stiffness coefficient (N/m)  
 $k$  cross-coupled stiffness coefficient (N/m)  
 $L$  length of the annular flow region (m)  
 $M$  direct added mass coefficient (kg)  
 $m$  cross-coupled added mass coefficient (kg)  
 $Re_{cir}$  circumferential velocity defined in Eqn. (6)  
 $r'$  radial position in  $x'o'z'$  frame (m)  
 $r_1$  radius of the rotor (m)  
 $r_2$  radius of the stator (m)  
 $t$  time (s)  
 $U(\eta, \phi)$  inlet velocity profile (m/s), Eqn. (7)  
 $U_a$  velocity compensation (m/s), Eqn. (8)  
 $U_p$  peripheral velocity of the rotor surface (m/s),  $U_p = \omega r_1$   
 $U_0$  velocity at center line in the cross-sectional plane (m/s)  
 $x$  displacement of the rotor center along  $x$ -axis (m)

- $z$  displacement of the rotor center along  $z$ -axis (m)
- $\delta$  half width of inlet region (m),  $\delta = 0.5H$ , in Eqn. (7) and Eqn. (8)
- $\eta$  radial position (m),  $\eta = r' - r_1$ , in Eqn. (7) and Eqn. (8)
- $\mu$  viscosity of fluid (Pa·s)
- $\rho$  density of fluid (kg/m<sup>3</sup>)
- $\phi$  angle measured in frame  $x'o'z'$  (rad), in Fig. 7
- $\Omega$  whirl speed of the rotor (rad/s)
- $\omega$  angular speed of the rotor (rad/s)

## INTRODUCTION

Canned motor pump is used as the reactor coolant pump (RCP) of pressurized water nuclear reactor (PWR). The canned motor RCP is a vertical rotor-bearing system with its entire shaft immersed in the reactor coolant, which is water for PWR. It is believed that, the annular flow between the rotor and the stator will substantially affect the rotordynamic characteristics of the RCP. It is required that the dynamic characteristics of RCP should be fully analyzed in the design stage to guarantee the functionality and, most importantly, safety during its long-time service. Therefore, a close investigation is needed to address the properties of the annular flow before any convincing results can be achieved from rotordynamic analysis of the canned motor RCPs.

Similar configuration of the annular flow between the rotor and stator of canned motor RCP can be found in bearings and seals. As in bearings and seals, the fluid of the annulus will exert dynamic force on the whirling rotor. And conventionally, the fluid force can be interpreted as certain dynamic coefficients, such as added mass, damping and stiffness [1].

Enormous work can be found in the literature in which researchers made efforts on obtaining the dynamic coefficients of the turbulent annular flow. It seems that, Fritz [2,3] is among the first who systematically studied the fluid force of turbulent annulus. For seals, Black and Jensen [4] were the first to try to model the dynamic coefficients. It is the brilliant work of Childs' [5] that successfully described the dynamic coefficients of turbulent seals with finite length. The theory of Childs is still developing and tested by lots of recent studies, like Migliorini et. al. [6]. Antunes et al. [7] developed a theoretical model which described the annular flow by 1-dimensional unsteady formulations. This theory was tested by experiments [8]. The theoretical models mentioned above are all based on the turbulent lubrication theories. Especially, Childs and Antunes et al. applied the so-called "bulk-flow theory" developed by Hirs [9] in the 1970s, which is based on the empirical relationship between the shear stresses and the circumferential Reynolds number. However, the circumferential Reynolds number of the canned motor RCP is usually too large to make the inertia effects become only first order terms as required in the bulk-flow theory. Thus, a more accurate model or technique is needed to reliably analyze the rotordynamic coefficients of annular flow of the canned motor RCP.

Unlike the theory mentioned above, CFD techniques make no assumptions on the relationship between the averaged circumferential velocity and the shear stresses on the surfaces of the rotor and the stator. Besides, CFD can handle the 3-dimensional nature of the annular flow if axial flow is present, like in canned motor RCPs. CFD analysis of annular flows generally falls into two categories, the steady-state and the unsteady-state simulations. For the steady-state simulations, the Single/Multiple Reference Frame (S/MRF) technique is often embraced [10, 11] to cope with the unsteady nature of the annular flow when whirl motion of the rotor is considered. In unsteady-state or transient simulations, the rotor actually whirls with its center follows certain orbit during the computation [12]. Generally, transient simulations consume much more computation time than the steady-state simulations. Up to 2011, Yan [13] reported that, approximately 360h was cost for a single case run of a transient simulation. It is observed that, once the force induced by fluid of the annular flow was calculated by CFD techniques, the dynamic coefficients could be obtained by certain curve fitting or regression method.

The aspect ratio (the ratio of the length to the diameter of the annular flow region,  $L/d$ ) of the canned motor RCP is relatively large compared to seals and bearings. In annular flow with large aspect ratio, the fluid induces dynamic moment on the rotor. Childs [14] suggested that the dynamic moment of the annular flow inside a seal with large aspect ratio should be modeled by the dynamic coefficients in matrix form with dimension of  $4 \times 4$ . Kanemori and Iwatsubo [15] analyzed the long annular flow inside a canned motor pump which had the similar structure of the canned motor RCP in question. Their results showed that the dynamic moment severely affected the rotordynamic characteristics of the pump. This analysis also suggested that the pre-swirl at the inlet of the annular flow is an important factor. Kanemori and Iwatsubo also studied the long annular flow by a series of experiments [16]. The experimental results confirmed that both the direct and the cross-coupled dynamic coefficients are the functions of the axial flow rate. Recently, Untaroiu et al. [17] performed numerical analysis of seals with large aspect ratio by CFD techniques. Significant difference was found between the results of CFD simulation and the predictions from theory. Untaroiu et al. claimed that this difference was the consequence of the relatively large aspect ratio of the annular flow.

As mentioned above, the pre-swirl at the inlet of annular flow is an important factor. Childs [5, 18] described the pre-swirl by the dimensionless inlet swirl parameter. This parameter was assumed to be within 0 to 0.5 for practical analysis. Recent study showed that high level of pre-swirl will increase the absolute value of cross-coupled stiffness coefficients [19]. Thus, the overall rotordynamic stability may degenerate when the pre-swirl is apparent. Therefore, the inlet pre-swirl level should be analyzed before any rotordynamic coefficients can be obtained.

In this work the CFD analysis are performed on two models. In the first model, the auxiliary impeller is modeled. The pre-

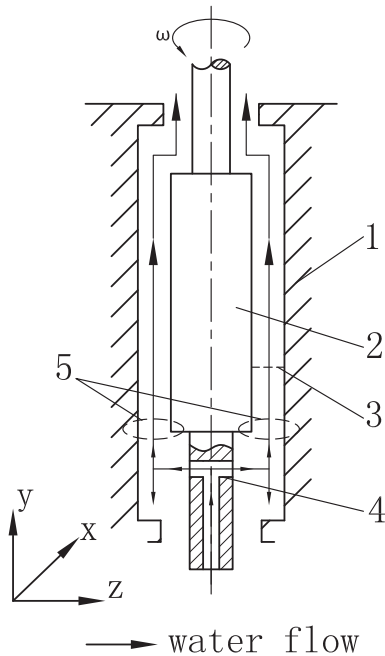


**FIGURE 1.** CONCEPTUAL DIAGRAM OF THE ANNULAR FLOW

1 - stator; 2 - rotor; 3 - clearance; 4 - auxiliary impeller; 5 - inlet region of the annular flow.

swirl level can be calculated with this model. In order to obtain the dynamic coefficients of the annular flow inside the canned motor RCP, the second model is built, which is a full scale model without the auxiliary impeller. The pre-swirl at the inlet is implemented by applying complex inlet boundary conditions. Simulations are carried out considering different axial flow rates. The dynamic coefficients are obtained and compared with the predictions of theory.

### ANALYSIS OF ANNULAR FLOW WITH THE AUXILIARY IMPELLER

As illustrated in Fig. 1, the canned motor RCP is a vertical pump system. The space between the rotor and stator is filled with reactor coolant (water), forming the region of the annular flow. The general geometry parameters of the present work are listed in Tab. 1. As shown in Fig. 1, the coolant water is propelled by the auxiliary impeller and flows spirally upwards in the clearance of the annular flow along the y-axis.

### Numerical Model

In order to deal with the complexity of the geometry, in Fig. 2, the fluid regions of the annular flow and the auxiliary impeller are divided into three domains and meshed by ANSYS

ICEM software. The flux of flow variables through adjacent domains is modeled by the non-conformal interface techniques provided by FLUENT software. Since the physical geometry of the fluid domain in question has a periodically repeating nature, and, due to limited computation hardware, 1/4 of the full scale flow region is modeled. The rotating-periodic boundaries are placed on the circumferential faces of the 1/4 model, as illustrated in Fig. 2. The periodic boundary technique is suitable for simulation on periodically repeating flow paths where the repeating flow patterns are expected. No additional pressure drop is brought by the periodic boundary and the flows across each pair of boundary planes are identical. These features make sure that the 1/4 model can reflect the flow properties of the full scale flow region. This method was also adopted in the studies of the flow fields in pumps and turbines, e.g. [20].

The rotating, unsteady nature of the annular flow with auxiliary impeller is transformed into a steady one by solving the fluid dynamics equations in the frame rotating with the same angular velocity of the rotor. This methodology is often referred as “Multiple Reference Frames (MRF)”. In fact, as indicated in Fig. 2, Domain A and Domain B are attached to the rotating frame while Domain C is attached to the non-rotating global frame.

The CFD simulations are performed with SST  $k - \omega$  turbulence model. This model was considered to exhibit better numerical stability than the  $k - \epsilon$  model [11]. The SIMPLE scheme is selected while the pressure, the momentum, the  $k$  and the  $\omega$  terms are all discretized by second order differencing. The convergence criteria for all the flow variables are set to be  $10^{-6}$ . The torque on the rotor along y direction is also monitored as convergence criterion. As illustrated in Fig. 3, the inlet boundary condition is set as pre-defined mass flow rate when the static pressure is set on the outlet. Special considerations are taken when handling the wall boundary conditions. To the authors’ knowledge, the inlet flow rate is approximately 700gpm (about 43.9 kg/s). The following simulations will be done with the axial flow under this baseline of mass flow rate. The walls of Domain A are set as stationary

**TABLE 1.** THE GEOMETRY PARAMETERS OF THE ANNULAR FLOW

Description	Quantity
Radius of rotor, $r_1$ (m)	0.29
Radius of stator, $r_2$ (m)	0.295
Length, $L$ (m)	2
Clearance, $h$ (mm)	5
Clearance ratio, $h/r_1$	0.017
Aspect ratio, $L/d$	3.45

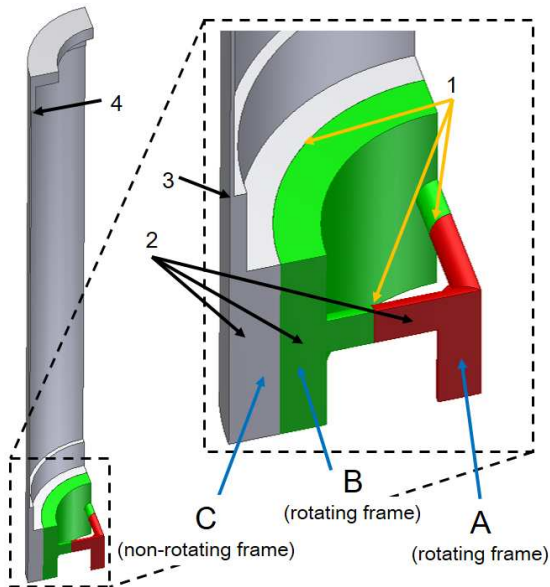


**FIGURE 2.** 1/4 MODEL

1 - interfaces; 2 - periodic boundaries; 3 - inlet of the annular flow; 4 - outlet of the annular flow.

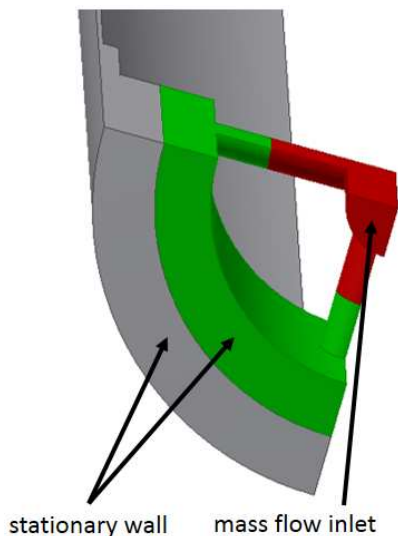


**FIGURE 3.** INLET AND WALLS

relative to the rotating frame. Therefore, the wall rotates with the same velocity of the rotor in the non-rotating global frame, which is denoted by  $\omega$ . For Domain B, the walls on the rotor is also set as stationary in the rotating frame while the wall away from the rotor surface is set to be stationary relative to the non-rotating global frame, as shown in Fig. 3. All the walls mentioned above are no-slip walls. For Domain C, since the referencing frame is non-rotating, the rotor wall is set as moving wall. The wall veloc-

ity is the same with the rotor angular velocity,  $\omega$ . The outer wall of Domain C, which is the inner surface of the stator, is set to be stationary no-slip wall. The parameters of the simulations are listed in Tab. 2. It is notable that, walls are placed at the bottom of Domain B and C. This treatment makes the CFD model to be different from the conceptual model depicted in Fig. 1. In fact, a portion of the coolant water propelled by the auxiliary impeller will flow downwards and re-circulate back to the impeller inlet. Due to the complexity of the re-circulating flow path, which goes through the bearings and other rotating components of the rotor, a numerical solution is inaccessible on the current computation hardware. However, this defect is assumed to have little effect on the final results since this work is mainly focused on the flow through the clearance between the rotor and stator.

**TABLE 2.** SIMULATION PARAMETERS OF THE MODEL WITH THE AUXILIARY IMPELLER

Description	Quantity
<b>Computation settings</b>	
Angular velocity of rotating frame (rad/s)	188.5
Wall rotating velocity of rotor surface (rad/s)	188.5
Mass flow rate at inlet (kg/s)	10.975
Initial pressure at inlet (Pa)	$1.55 \times 10^7$
Pressure at outlet (Pa)	$1.55 \times 10^7$
<b>Physical properties of the fluid</b>	
Density, $\rho$ (kg/m <sup>3</sup> )	994.7
Viscosity, $\mu$ (Pa · s)	$5.43 \times 10^{-4}$

Three sets of meshes are created to test the dependence of the numerical simulation on the mesh. The result is illustrated in Fig. 4. Detailed information of the final computation mesh with the largest number of cells is listed in Tab. 4. The meshed model is shown in Fig. 14, 15 and 16.

## Numerical Results

Particular attention is paid on the circumferential velocity ( $U$ ) of the fluid of the annular flow. Figure 5 (a) and (b) show the velocity profiles at the locations near the inlet and the outlet of the annular flow, respectively. The vectors of velocity in these figures are the velocity in the global stationary frame and projected to the cross-sectional plane. It is clear that, the fluid at the inlet of the annular flow gains its circumferential velocity as the consequence of the rotation of the auxiliary impeller.

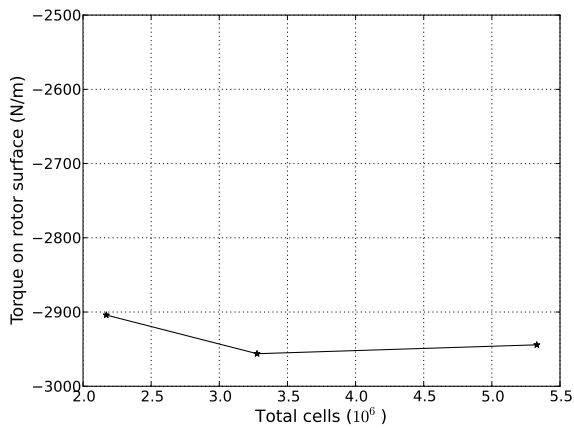


**FIGURE 4.** RESULT OF MESH DEPENDENCE TEST

The annular flow region has enough axial length for the flow to evolve and finally reaches the fully developed condition. This is shown in Fig. 6, in which the circumferential velocity along the line parallel to the  $y$ -axis and originates from the radial center of the clearance is depicted. In Fig. 5 and Fig. 6, one can see that near the outlet of the annular flow the circumferential velocity at the radial center of the cross-section,  $U_0$ , is 26.8m/s, approximately half (49%) the peripheral velocity of the rotor surface,  $U_p$ . It is the velocity at the inlet region of the annular flow that is worth further consideration, because it shows the inlet pre-swirl level of the annular flow.

The fluid may experience velocity fluctuation when flow into the annular region from relatively wide space. This could be found in Fig. 6 at the place where the non-dimensional axial location is small. Therefore, the pre-swirl velocity ratio ( $U_0/U_p$ ) for the annular flow in question could be obtained from the velocity profile slightly away from the inlet location. For the simulations in the following section, the non-dimensional pre-swirl ratio is set to be 0.36, which is obtained at the point with non-dimensional axial coordinate of 0.02 in Fig. 6.

## ANALYSIS OF THE ROTORDYNAMIC COEFFICIENTS

It is common practice to model the forces produced by the fluid of the annular flow by estimating dynamic pressure distribution on the rotor surface under the small perturbation assumption. This methodology is well established in analysis of annular flow of bearings and seals [17]. Thus, in order to obtain the rotordynamic coefficients of the annular flow of canned motor RCP, the rotor is assumed to whirl along a circular orbit with constant radius. The radius of the orbit is expressed by the eccentricity  $e$  of the center of the rotor under normal operating condition, as shown in Fig. 7. Although, the bending displacement of the rotor along the  $y$ -axis and the misalignment of the rotor-bearing sys-

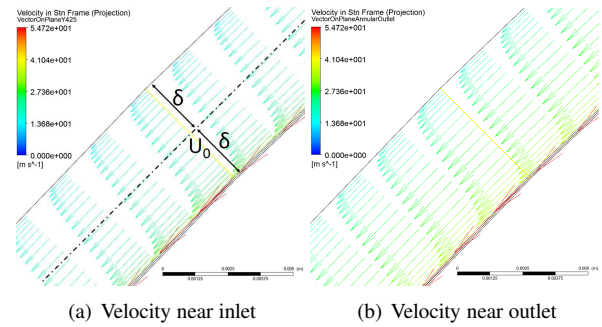


**FIGURE 5.** VELOCITY PROFILES  
The dash-dot line is the center line of the cross-sectional plane.

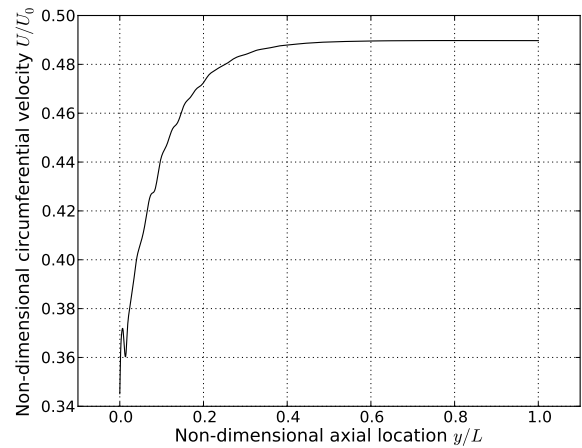


**FIGURE 6.** CIRCUMFERENTIAL VELOCITY ALONG Y-AXIS

tem can affect the dynamic behavior of the canned motor RCP, for the present work, they are not considered.

## Rotordynamic Coefficients of the Annular Flow

Suppose the global stationary frame,  $xoz$ , is attached to the stator. There is a rotating frame,  $x'o'z'$ , attached to the rotor with the origin at the rotor center, as illustrated in Fig. 7. The rotor is whirling with eccentricity  $e$ . The angle between the two frame is denoted by  $\Omega t$ , where  $\Omega$  is the angular speed of the whirl motion. Conventionally, the dynamic forces of the annular flow can be modeled by the ordinary differential equations Eqn. (1).

$$\begin{Bmatrix} F_x \\ F_z \end{Bmatrix} = - \begin{bmatrix} M & m \\ -m & M \end{bmatrix} \begin{Bmatrix} \ddot{x} \\ \ddot{z} \end{Bmatrix} - \begin{bmatrix} C & c \\ -c & C \end{bmatrix} \begin{Bmatrix} \dot{x} \\ \dot{z} \end{Bmatrix} - \begin{bmatrix} K & k \\ -k & K \end{bmatrix} \begin{Bmatrix} x \\ z \end{Bmatrix} \quad (1)$$

where  $F_x$  and  $F_z$  are the fluid induced forces along  $x$  and  $z$  axes. In Eqn. (1),  $M$  and  $m$  are the direct and cross-coupled coefficients of

added mass, respectively. Similarly, the direct and cross-coupled coefficients of damping and stiffness are expressed by the  $C_s$  and  $K_s$ . Since the rotor is whirling along the circular orbit with whirl speed of  $\Omega$ , the location of the rotor center  $o'$  at specific time  $t$  can be expressed as:

$$\begin{Bmatrix} x \\ z \end{Bmatrix} = e \begin{Bmatrix} \cos \Omega t \\ -\sin \Omega t \end{Bmatrix} \quad (2)$$

The force components  $F_x$  and  $F_z$  can be written in terms of the normal component  $f_n$  and tangential component  $f_t$  in the rotating frame  $x'o'z'$ . In this frame,  $f_n$  is parallel to  $o'x'$  while  $f_t$  is always ahead of  $f_n$  with the angle of  $\pi/2$ . It is easy to derive the expressions of  $F_x$  and  $F_z$  in terms of  $f_n$  and  $f_t$ .

$$\begin{cases} F_x = f_n \cos \Omega t - f_t \sin \Omega t \\ F_z = -f_n \sin \Omega t - f_t \cos \Omega t \end{cases} \quad (3)$$

Substitute Eqn. (2) and Eqn. (3) into Eqn. (1), and solve for  $f_n$  and  $f_t$ . The result is as follows:

$$\frac{1}{e} \begin{Bmatrix} f_n \\ f_t \end{Bmatrix} = \begin{Bmatrix} M\Omega^2 + c\Omega - K \\ m\Omega^2 - C\Omega - k \end{Bmatrix} \quad (4)$$

At this point, the approximations of the rotordynamic coefficients could be obtained through the curve fitting approach when the force components,  $f_n$  and  $f_t$ , are calculated with several whirl speeds. The above methodology is utilized in lots of work, e.g. [17].

It is notable that, in Eqn. (2), the negative sign in the expression of  $z$  is the consequence of right-hand rule of rotation in  $y$  direction. The orientation of the coordinate system is selected simply because the CFD simulation is performed in this way. It should be bearing in mind that when comparing the results of the present work obtained from Eqn. (4) with the results found in the literature, the cross-coupled values of the rotordynamic coefficients will have the opposite signs.

### Numerical Model without the Auxiliary Impeller

It is obvious that, in order to obtain the rotordynamic coefficients through Eqn. (4), the force components should be calculated in the rotating frame. At the same time, certain amount of eccentricity have to be modeled. Therefore, the whole fluid region should be meshed instead a portion of it. Based on the numerical results of the pre-swirl inside the canned motor RCP and the limitation of computation hardware, the eccentric model

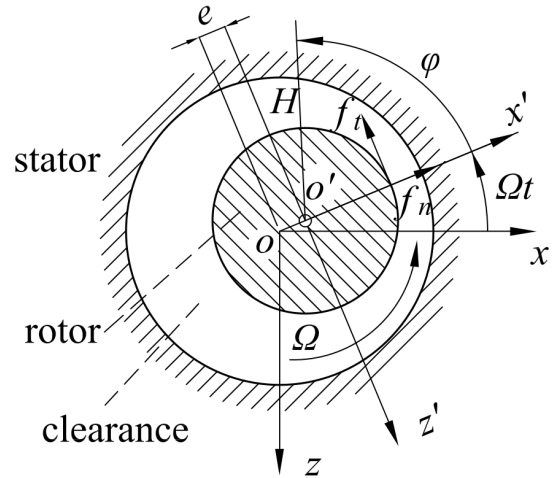


FIGURE 7. WHIRL MOTION OF THE ROTOR

is built without the auxiliary impeller. The fluid region is modeled by the space between two cylindrical surfaces. The ratio of eccentricity ( $e$ ) and the clearance between the two cylinders ( $h$ ) is 0.1. This value is usually used in the analysis of annular seals [17].

Similar to the techniques used in the simulation of the model with auxiliary impeller, the entire fluid domain is attached to the rotating frame,  $x'o'z'$ . The velocities of both the inner and outer walls are specified relative to the angular velocity of the rotating frame. The rotating frame rotates about the origin of frame  $xoz$  with the pre-defined whirl speed. The inner wall (surface of rotor) rotates about the origin of  $x'o'z'$  with angular velocities defined respect to the rotating frame. It should be satisfied that, when referred to the global stationary frame, the velocities of the inner and the outer walls must be  $\omega$  and zero, respectively. Here,  $\omega$  is the rotation speed of the rotor. It is convenient to take the angle  $\Omega t$  in Fig. 7 as zero when this rotating frame method is adopted. Then the eccentricity is along the  $x$ -axis in  $xoz$  frame since the  $o'x'$  axis is parallel to the  $ox$  axis. Consequently, the forces in  $x$  and  $z$  direction calculated in the  $xoz$  frame are the  $f_n$  and  $f_t$  required in Eqn. (4).

The pre-swirl effect is achieved by imposing complex boundary condition on the inlet of the annular flow. The clearance  $H$  is the function of the angle,  $\phi$ , measured from the  $x'$ -axis in the frame  $x'o'z'$ .  $H$  is approximated by Eqn. (5) provided that  $e$  is much smaller than  $r_1$  [5].

$$H = h - e \cdot \cos \phi \quad (5)$$

where  $h$  is the nominal clearance of the annular flow. The steady-state velocity profile on the cross-sectional plane near the inlet of the annular flow is shown in Fig. 5(a) in the previous section.

Turbulent flow can be expected if we calculate the local circumferential Reynolds number by Eqn. (6) with the center velocity  $U_0$  shown in Fig. 5.

$$Re_{cir} = \frac{\rho U_0 H}{\mu} \quad (6)$$

For the present work, the  $Re_{cir}$  is over  $1 \times 10^4$  after evaluation of Eqn. (6) with the  $U_0$  of 0.36 pre-swirl ratio. Since the flow can be considered as turbulent, the velocity profile near the inlet of the annular flow can be approximated by the log-law distribution. In Fig. 5, the circumferential velocity on the cross-sectional plane is divided into two parts with respect to the center line. At specific  $\phi$ , the radial width of each divided part is  $\delta(\phi) = 0.5H(\phi)$ . In frame  $x'o'z'$ , let  $r'$  be the radius of a point locating in the annular flow. The log-law distribution is achieved by comparing  $r' - r_1$  and  $\delta$ . Let  $\eta = r' - r_1$ . Equation (7) describes the velocity profile,  $U(\eta, \phi)$ :

$$U(\eta, \phi) = \begin{cases} U_0 \left( \frac{H-\eta}{\delta} \right)^{\frac{1}{7}} & \eta > \delta \\ 2U_0 - U_0 \left( \frac{\eta}{\delta} \right)^{\frac{1}{7}} + U_a(\eta, \phi) & \eta \leq \delta \end{cases} \quad (7)$$

where

$$U_a(\eta, \phi) = \left( 1 - \left( \frac{\eta}{\delta} \right)^{\frac{1}{7}} \right) (U_p - 2U_0) \quad (8)$$

In Eqn. (7),  $U_p = \omega r_1$  is the peripheral velocity of the rotor surface. For the case of  $\eta > \delta$ , the velocity of the fluid approaches zero because the wall of the stator is not rotating. However, for the case of  $\eta \leq \delta$ , the formulation is different. It is clear that the velocity  $U_0$  at the center line of the cross-sectional plane is not from the fully developed flow region. Therefore, certain terms have to be added into the log-law formulation. This is done by  $U_a$  in Eqn. (7) with  $\eta \leq \delta$ . The formulation of  $U_a$  is a kind of compensation and is not theoretically testified yet. The profiles of the inlet flow shown in Fig. 5(a) and from the approximation by Eqn. (7) are compared in Fig. 8. The divergence between them is assumed to have little effect on the final results. The implementation of the inlet boundary condition is done by the help of the UDF functionality of FLUENT.

The turbulence model and discretization schemes are the same with the simulation in the previous section. The relationship between the axial flow and the rotordynamic coefficients are studied by setting various inlet mass flow rates. There are 5 distinct flow rates from 0 to 700gpm. In order to get the rotordynamic coefficients, 5 whirl ratios are selected. Appropriate

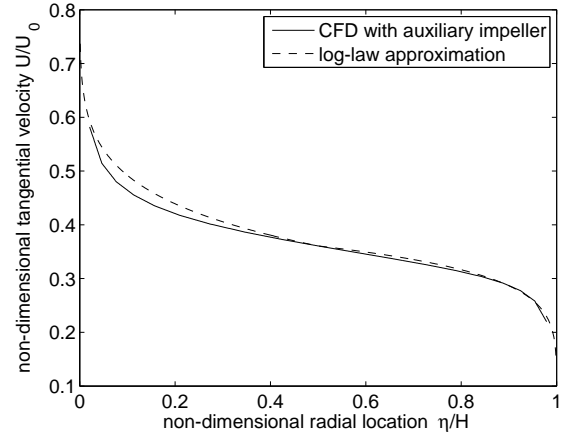


FIGURE 8. LOG-LAW APPROXIMATION AT THE INLET

frame rotating speeds and associated wall speeds are configured accordingly. 25 simulations are performed with the combined inlet mass flow rates and the whirl speeds. The detailed parameters for the simulations are listed in Tab. 3.

TABLE 3. PARAMETERS OF SIMULATION WITHOUT THE AUXILIARY IMPELLER

Description	Quantity
Eccentricity, $e$ (mm)	0.5
Inlet mass flow rates (kg/s)	0, 10.975, 21.95, 32.925, 43.9
Angular speed of rotor, $\omega$ (rad/s)	188.5
Whirl ratio, $\Omega/\omega$	0, 0.25, 0.5, 0.75, 1
Pre-swirl ratio, $U_0/U_p$	0.36

## Results and discussion

For each simulation, the forces along x and z axes are obtained by the integration of pressure over the rotor surface. The curves in Fig. 9 and Fig. 10 show the relationship between the forces and the whirl ratios of the rotor under different axial mass flow rates. The force predictions by Fritz's theory are also drawn in these two figures. The formulation of the theory is the same with that provided by Brennen [1]. Particularly, for the calculation of the theoretical prediction, the friction factor is obtained from the well known Prandtl's friction law for smooth pipes [21] and the correlation between the friction factors of the pipe and

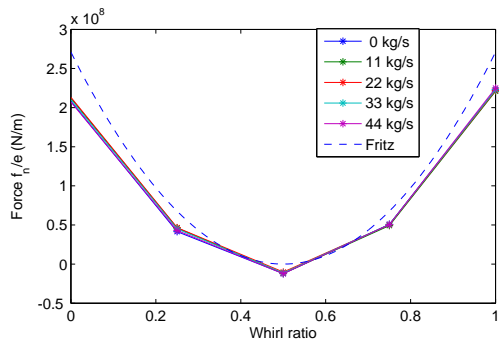


FIGURE 9.  $f_n$  COMPONENT OF THE FORCE

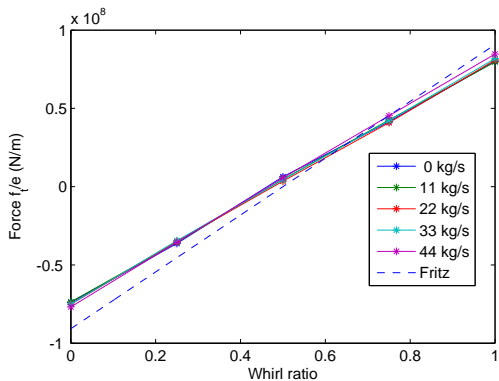


FIGURE 10.  $f_t$  COMPONENT OF THE FORCE

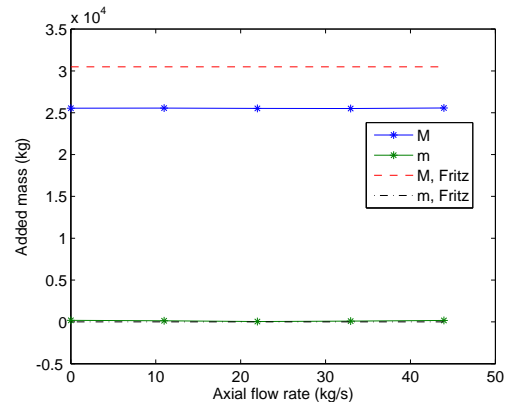


FIGURE 11. ADDED MASS WITH PRE-SWIRL RATIO 0.36

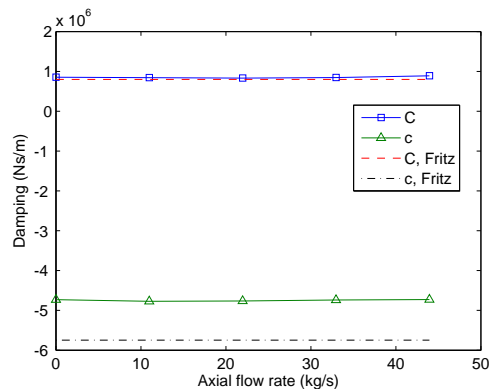


FIGURE 12. DAMPING WITH PRE-SWIRL RATIO 0.36

the turbulent concentric annular flow [16].

The normal force component  $f_n$  does exhibit the relationship approximated by Eqn. (4). However, the tangential force component  $f_t$  appears to be linear within the range of whirl ratios studied. The similar curve was obtained by Untaroiu et al. [17]. The tangential force is relatively small compared with the normal force. However, these two force components both have their minimum absolute value near the point of 0.5 whirl ratio. The tangential force acts as the destabilizing factor with whirl ratio under 0.5, since the force is along the negative  $z$  direction, which is the same direction of the whirl motion. These phenomena were also reported by Kanemori et al. [16] from experiments. It is easy to observe that, in almost all the range of whirl ratios, the direction of dominant  $f_n$  component is along the positive  $x$ -axis and destabilizes the rotor system, except when whirl ratio is near 0.5.

It is clear that the forces vary slightly with respect to the axial flow rates for the present work. Therefore, the dynamic characteristics will be hardly effected by the axial flow rates under 700gpm. However, it should be noted that, this result is under the assumption of constant pre-swirl ratio, which is obtained from the simulation with the auxiliary impeller modeled. In other words, the inlet pre-swirl and the axial flow rate are assumed to

be non-coupled.

The rotordynamic coefficients of added mass, damping and stiffness are illustrated in Fig. 11, Fig. 12 and Fig. 13, respectively. Both direct and cross-coupled coefficients are shown. The predictions of Fritz's theory are also indicated in the figures by horizontal lines since the theory does not take axial flow rate into consideration. Large divergence between the results of CFD and theory are found. Untaroiu et al. [17] reported the similar situation. They argued that these differences between CFD and theory may attributed to the large aspect ratio of the annular flow region. As expected from the force components, the direct stiffness of the annular flow is negative, which could be recognized as the sign of destabilizing effect. It is clear that the annular flow brings substantial added mass into the rotordynamic system. The results of CFD simulation suggest that the effects of annular flow should be considered in the rotordynamic analysis to obtain accurate predictions of the dynamic characteristics of the canned motor RCP.

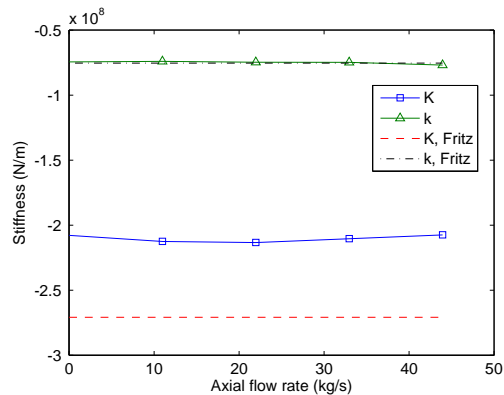


FIGURE 13. STIFFNESS WITH PRE-SWIRL RATIO 0.36

## CONCLUSION

In this study, two CFD simulations are performed for the annular flow inside the canned motor RCP. The inlet pre-swirl level is obtained from the model with the auxiliary impeller. The fluid induced forces of different whirl speeds and axial flow rates are calculated with constant pre-swirl level. The rotordynamic coefficients of the annular flow under different axial flow rates are obtained. These coefficients are slightly affected by the axial flow rates with the current pre-swirl condition. The direct stiffness of the annular flow is found to be negative. Substantial added mass is brought by the annular flow into the rotordynamic system. The annular flow has significant effects on the dynamic characteristics of the canned motor RCP. Therefore, the annular flow should be considered in the analysis of the rotor bearing system to achieve accurate predictions for the canned motor RCPs.

## ACKNOWLEDGMENT

This research work was funded by China Postdoctoral Science Foundation (2013M531173) and Shanghai Postdoctoral Science Foundation (13R21414100).

## REFERENCES

- [1] Brennen, C. E., 2011. *Hydrodynamics of pumps*. Cambridge University Press.
- [2] Fritz, R., 1970. "The effects of an annular fluid on the vibrations of a long rotor, part 1theory". *Journal of Basic Engineering*, **92**, p. 923.
- [3] Fritz, R., 1970. "The effects of an annular fluid on the vibrations of a long rotor, part 2test". *Journal of Basic Engineering*, **92**, p. 930.
- [4] Black, H., and Jensen, D., 1970. "Dynamic hybrid properties of annular pressure seals". *Proc. J. Mech. Eng.*, **184**, pp. 92–100.
- [5] Childs, D. W., 1983. "Finite-length solutions for rotordynamic coefficients of turbulent annular seals". *Journal of lubrication technology*, **105**, p. 437.
- [6] Migliorini, P. J., Untaroiu, A., Wood, H. G., and Allaire, P. E., 2012. "A computational fluid dynamics/bulk-flow hybrid method for determining rotordynamic coefficients of annular gas seals". *Journal of Tribology*, **134**, pp. 022202–1–022202–9.
- [7] Antunes, J., Axisa, F., and Grunenwald, T., 1996. "Dynamics of rotors immersed in eccentric annular flow. part 1: Theory". *Journal of Fluids and Structures*, **10**(8), pp. 893–918.
- [8] Grunenwald, T., Axisa, F., Bennett, G., and Antunes, J., 1996. "Dynamics of rotors immersed in eccentric annular flow. part 2: experiments". *Journal of fluids and structures*, **10**(8), pp. 919–944.
- [9] Hirs, G. G., 1970. "Fundamentals of a bulk-flow theory for turbulent lubricant films". PhD thesis, Technische Hoogeschool te Delft.
- [10] Moore, J. J., 2003. "Three-dimensional cfd rotordynamic analysis of gas labyrinth seals". *Journal of vibration and acoustics*, **125**(4), pp. 427–433.
- [11] Untaroiu, A., Hayrapetian, V., Untaroiu, C. D., Wood, H. G., Schiavello, B., and McGuire, J., 2013. "On the dynamic properties of pump liquid seals". *Journal of Fluids Engineering*, **135**, pp. 051104–1–051104–10.
- [12] Sekaran, A., and Morrison, G., 2010. "Study of the impact of change of clearance on the flow field and rotordynamic coefficients for a smooth, whirling annular seal". In Proceedings of the ASME 2010 3rd Joint US-European Fluids Engineering Summer Meeting, ASME.
- [13] Yan, X., Li, J., and Feng, Z., 2011. "Investigations on the rotordynamic characteristics of a hole-pattern seal using transient cfd and periodic circular orbit model". *Journal of vibration and acoustics*, **133**(4).
- [14] Childs, D. W., 1982. "Rotordynamic moment coefficients for finite length turbulent seals". In Proceedings of the IFToMM Conference, Rome, pp. 371–378.
- [15] Kanemori, Y., and Iwatsubo, T., 1994. "Rotordynamic analysis of submerged motor pumps: Influence of long seal on the stability of fluid machinery.". *JSME International Journal. Ser. C, Dynamics, control, robotics, design and manufacturing*, **37**, pp. 193–201.
- [16] Kanemori, Y., and Iwatsubo, T., 1992. "Experimental study of dynamic fluid forces and moments for a long annular seal". *Journal of Tribology*, **114**, pp. 773–778.
- [17] Untaroiu, A., Untaroiu, C. D., Wood, H. G., and Allaire, P. E., 2013. "Numerical modeling of fluid-induced rotordynamic forces in seals with large aspect ratios". *Journal of Engineering for Gas Turbines and Power*, **135**(1), pp. 012501–012501.
- [18] Childs, D. W., 1983. "Dynamic analysis of turbulent annular seals based on hirs lubrication equation". *Journal of*

*lubrication technology*, **105**, p. 429.

- [19] Kirk, G., and Gao, R., 2012. "Influence of preswirl on rotordynamic characteristics of labyrinth seals". *Tribology Transactions*, **55**(3), pp. 357–364.
- [20] Rao, V. N., Tucker, P., Jefferson-Loveday, R., and Coull, J., 2013. "Large eddy simulations in low-pressure turbines: Effect of wakes at elevated free-stream turbulence". *International Journal of Heat and Fluid Flow*, **43**(0), pp. 85 – 95.
- [21] Pope, S. B., 2000. *Turbulent flows*. Cambridge university press.

**Appendix A: Mesh Information of the Model with the Auxiliary Impeller**

The pictures of the final meshed model of the domains indicated in Fig. 2 are shown in Fig. 14, Fig. 15 and Fig. 16. Other information of the final meshed model is listed in Tab. 4.

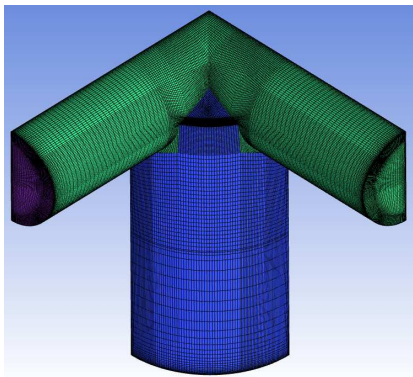


**FIGURE 14.** MESH OF DOMAIN A

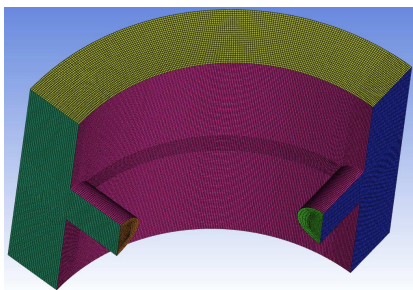


**FIGURE 15.** MESH OF DOMAIN B

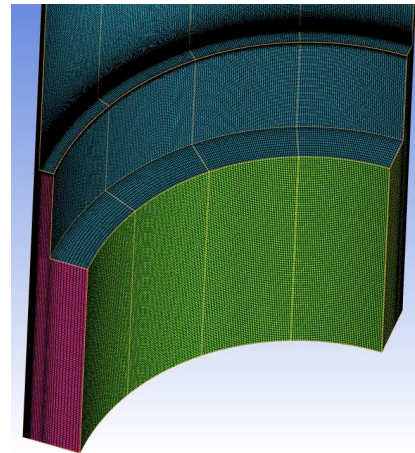


**FIGURE 16.** MESH OF DOMAIN C

**TABLE 4.** MESH INFORMATION OF THE MODEL WITH AUXILIARY IMPELLER

Meshed Domain	Nodes	Hexahedra
Domain A	776385	748096
Domain B	917233	874240
Domain C	3865037	3707392